GEOPHYSICS®

Monitoring subsurface changes by tracking direct-wave amplitudes and traveltimes in continuous DAS VSP data

Journal:	*Geophysics*
Manuscript ID	GEO-2021-0404.R1
Manuscript Type:	Letters
Keywords:	DAS (distributed acoustic sensors), attributes, 4D, borehole geophysics, monitoring
Manuscript Focus Area:	Geophysics Letters

Monitoring subsurface changes by tracking direct-wave amplitudes and traveltimes in continuous DAS VSP data

Running head: Monitoring with traveltimes and amplitudes

Roman Pevzner[1], Stanislav Glubokovskikh[1,2], Roman Isaenkov[1], Pavel Shashkin[1], Konstantin Tertyshnikov[1], Sinem Yavuz[1], Boris Gurevich[1] , Julia Correa[2], Todd Wood[2] and Barry Freifeld[3]

[1]Curtin University, GPO Box U1987, Perth 6845, Western Australia

[2]Lawrence Berkeley National Laboratory, 1 Cyclotron Road, MS 74R-316C, Berkeley, CA, USA, 94720

[3]Class VI Solutions, Inc., 711 Jean St., Oakland, CA, USA, 94610

Corresponding author: Pavel Shashkin pavel.shashkin@curtin.edu.au

Abstract

Instrumenting wells with distributed acoustic sensors (DAS) and illuminating them with passive or active seismic sources allows precise tracking of temporal variations of direct-wave traveltimes and amplitudes, which can be used to monitor variations in formation stiffness and density. This approach has been tested by tracking direct-wave amplitudes and traveltimes as part of a CCS project where a 15 kt supercritical CO_2 injection was monitored with continuous offset VSPs using nine permanently mounted surface orbital vibrators (SOVs) acting as seismic sources and several wells instrumented with DAS cables cemented behind the casing. The results show a significant (from 15 to 30%) increase of strain amplitudes within the CO_2 injection interval, and traveltime shifts of 0.3 to 0.4 ms below this interval, consistent with full-wave 1.5D numerical simulations and theoretical predictions. The results give independent estimates of the CO_2 plume thickness and the associated P-wave velocity reduction.

Introduction

Permanent or on-demand seismic monitoring (PSM) is increasingly used for subsurface surveillance in a variety of applications, such as oil & gas production, CO_2 geosequestration, and geothermal production, to name a few (Cheng et al., 2021; Davies et al., 2020; Zhu et al., 2019; Zwartjes et al., 2015). Most monitoring solutions employ time-lapse (4D) reflection seismic methodology. Reflection seismology for subsurface characterization often benefits from complementary borehole seismic studies, such as vertical seismic profiling (VSP). The principal benefit of VSP is placement of seismic receivers (or sources) within the target formation or in its immediate vicinity, which allows in-situ calibration of the reflected seismic wavefield (Galperin and White, 1974). However, such a calibration is largely impractical for time-lapse applications, as it is challenging if not impossible to place conventional VSP tools in wells for years or decades.

This technological challenge can be addressed by replacing standard seismic receivers (geophones, hydrophones) with fiber-optic cables installed in or along boreholes. Fiber-optic cables used as distributed acoustic sensors (DAS) measure axial strain (or strain rate) along the fiber, providing data quality comparable or superior to geophones, and can cover an entire length of the well (rather than the typical 100 m to 200 m spanned by a geophone-based VSP tool) (Daley et al., 2013; Mateeva et al., 2017; Naldrett, 2021; Parker et al., 2014). Once installed, DAS can be used for continuous seismic monitoring using permanently installed seismic sources, or for on-demand monitoring using mobile seismic sources such as vibroseis. Alternatively, DAS allows continuous monitoring in passive mode, using natural or made-made sources such as earthquakes or anthropogenic noise. One such application was proposed by Pevzner et al., (2020), who showed that the direct wave strain amplitude measured by DAS can be used to monitor the changes in elastic formation properties in the vicinity of the wellbore. The same dependence of the amplitude on stiffness can also be used to calibrate DAS depth against well log data (Mateeva and Zwartjes, 2017)

In this study we use the amplitude and traveltime attributes of the direct wave measured by DAS to monitor a small injection of CO_2 into an aquifer. Placing the receivers immediately above and below the injection interval allows precise estimation of sub-millisecond traveltime shifts, while amplitude variations measured by receivers inside the reservoir carry information about the changes in both velocity and density.

Theory

When a plane P-wave propagating along a well passes through a formation, it induces dynamic strain that is related to the stiffness of the formation: the softer the formation, the larger the strain. As shown by Pevzner et al., (2020), when transmission losses within one wavelength are small, the induced axial strain amplitude ϵ is approximately proportional to the quantity

$$\epsilon = \left(\rho V_P^3\right)^{-1/2}, \tag{1}$$

where ρ is formation density and V_P is P-wave velocity. It follows that variations of velocity or density over time should cause temporal variations in the strain amplitude. Even when transmission losses are significant (i.e., in the vicinity of sharp interfaces), the strain amplitudes could be distorted, but temporal variations of $\left(\rho V_P^3\right)^{-1/2}$ can still be estimated from temporal variations in ϵ.

In addition to amplitude changes, temporal changes of the formation velocity (which could happen without change in density!) will change the direct-wave traveltimes below that formation. If the velocity V_P in a target formation of thickness h has increased by a small increment, ΔV_P, then the traveltimes before and after the changes are h/V_P and $h/(V_P + \Delta V_P)$, respectively, and thus the traveltime shift caused by these changes is

$$\Delta t = \frac{h}{(V_P + \Delta V_P)} - \frac{h}{V_P} = -\frac{h\Delta V_P}{(V_P + \Delta V_P)V_P} \cong -\frac{h\Delta V_P}{V_P^2}. \quad (2)$$

Field experiment

Direct-wave amplitudes and traveltimes were measured as part of a CCS project, where a small CO_2 injection was monitored with continuous offset VSPs using nine permanently mounted surface orbital vibrators (SOVs) acting as seismic sources(Correa et al., 2021; Freifeld et al., 2016; Pevzner et al., 2021) and several wells instrumented with fiber-optic DAS cables cemented behind the casing acting as receivers (Figure 1). In this experiment, 15 kt of CO_2 was injected between 12 January, 2020 through 16 April, 2021through the CRC-3 well into a saline aquifer located roughly 1,550 m below the surface. CRC-3 was drilled to a depth of 1640 m and is instrumented with a DAS cable with enhanced backscattering fiber installed from surface to the total depth (Correa et al., 2017). The well is perforated between 1536-1547 m. CRC-3 is the only well penetrating the expected CO_2 plume and thus in this paper we use measurements from this well only.

DAS data are acquired continuously with 1 kHz sampling rate and have accurate GPS time stamps. The SOVs are operating sequentially for 2.5 hours each day, with a single full vintage for all nine SOVs acquired every 48 hours. Individual sweeps (half – clockwise (CW), half – counterclockwise (CCW)) are extracted from DAS records using data from a GPS time-synchronized reference geophone deployed 3 m beneath the SOV (Isaenkov et al., 2021).

The DAS-SOV VSP has been recording from 06 June 2020. Here we analyze data acquired until late May 2021.

Amplitude variations and traveltime shifts

Details of the processing flow for DAS/SOV data are given in Yavuz et al., (2020) and Isaenkov et al., (2021). Here we provide a short overview of the data preprocessing necessary for measuring traveltimes and amplitudes. The same workflow is used for all SOVs.

For each vintage, we deconvolve individual sweeps extracted from DAS data initially with the nearfield record of the reference geophone. At this stage, CW and CCW sweeps within the vintage are stacked separately for each direction.

Then, the source signature is extracted from the direct-wave DAS VSP record (far field record) and the data is deconvolved with this extracted wavelet for each rotation direction. This procedure produces a wavelet that is close to zero-phase and is very stable. Stacking the CW and CCW records suppresses shear wave energy, resulting in data representing a vertically polarized seismic source.

First breaks are picked automatically along the main peak of the zero-phase wavelet and stored as a function of receiver depth and vintage. Prior to this procedure, the data are resampled to a finer sampling rate of 0.05 ms using zero padding in the frequency domain (Smith, 2007), which corresponds to accurate reconstruction of a band-limited time series. Peak amplitudes are also measured using the interpolated data.

To analyze the traveltime shifts caused by injection on a single SOV data vintage, we perform the following steps:

- All traveltime functions for vintages acquired prior to the injection are averaged for each receiver depth and represent the 'baseline.' Although there are up to ~1 ms discrepancies between the vintages, these are random and this procedure gives a robust estimate;

- The 'baseline' is subtracted from all the individual vintages (both acquired before and after the start of injection) to form de-trended traveltimes.
- To remove remaining vintage-to-vintage jitter, we average (alpha-trimmed with 50% cut-off) detrended traveltimes over the receivers located at least 100 m above the injection interval for each vintage and subtract these residuals.

The result of this procedure for all SOVs is presented in Figure 2 (left plots) for the bottom section of the well. The perforation interval is shown with horizontal dashed lines and the start of injection is marked with the vertical dashed blue line. The injection-related traveltime shifts are observed to occur from the very start of the injection. All the vintages after the completion of injection are averaged and plotted as a black line on the right panels in comparison with traveltime shifts obtained from simulations (as discussed below).

Peak amplitudes are processed similarly. First, we estimate the baseline amplitude, and then use it to obtain amplitude variations by subtracting the baseline from each vintage. Deconvolution normalizes the wavelet amplitude, and as such, there is no need for further filtering. Thus, the relative amplitude change is computed by dividing the amplitude variations on individual vintages by the baseline amplitude. The relative amplitude variations are shown in figure 3.

Numerical simulations

To better understand the results, we perform time-lapse 1.5D full-wave numerical simulations with OASES software (Schmidt and Jensen, 1985), which models 3D wave propagation in a 1D stratified (1D) medium. In the baseline models, the velocity and density of all layers are obtained from sonic and density logs. For the monitor model, the effect of injected CO_2 is estimated using the Gassmann-Wood uniform saturation model (Caspari et al., 2015; Johnson, 2001; Mavko and Mukerji, 1998), assuming a CO_2 saturation in the injection interval (at the end of injection) of 10%. This calculation estimates a reduction of the P-wave velocity in the reservoir of ~300 m/s. The seismograms are computed with the source wavelets extracted from field data at the target horizon (Isaenkov et al., 2021). The same workflow that was applied to the field data was applied to synthetic data to compute traveltime shifts and amplitudes for an assumed CO_2 thickness which was varied from 0 to 20 m. The results for an 11 m thick plume (red lines in the right panels of Figures 2 and 3) show good agreement with field data (black lines), with some notable differences discussed below. The thickness of 11 m, which produces the best match between the data and modeling, is consistent with the length of the perforation interval but slightly thinner than the average result of flow simulations, which vary between 10 and 15 m, depending on the model realization (Jenkins et al., 2021).

Analysis of the results

Both field and modeled traveltime shifts in the right panels of Figure 3 show similar increases within and below the plume (corresponding to a decrease of velocity caused by CO_2 saturation), preceded by a small decline, likely due to interference with reflected waves. Below the injection interval (shown with dashed lines in the left panels), the modeled traveltime shifts remain nearly constant with increasing depth, whereas the traveltime shifts computed from field data gradually decline. This is likely the result of the finite lateral dimensions of the plume causing diffraction of the direct waves around the plume edges. The contour of the plume modeled with flow simulations is shown as a red line in Figure 1. Indeed, the decline of the traveltime shifts is the strongest for SOV6 located to the south-west of CRC-3, where the lateral spread of the plume is the smallest.

Conversely, the observed traveltime shifts remain almost constant (with depth) for SOV5 and SOV7 located to the south-east of CRC-3; in the direction the plume is predicted to migrate further.

The observed amplitude variation is also consistent with the modeling (in the right panels of Figure 2), with a notable exception of a decline of field amplitudes below the reservoir. The nature of this effect is not entirely clear. It may be related to some filtering implemented in the DAS equipment, or vertical heterogeneity of the CO_2 saturation within the plume, as the modeling was done assuming constant saturation of 10%, which is a crude approximation. The latter effect can be modeled, but requires knowledge of the fine-scale structure of the CO_2 plume (Caspari et al., 2015).

From equation 1, the expected reduction of velocity by $\Delta V_P = 300$ m/s gives a strain amplitude increase within the reservoir of ~15%, which is consistent with the modeling for the zero-offset VSP (SOV3) but underestimates the reduction of the field amplitude. Note that the formation density change for such a small saturation is negligible. Furthermore, the modeling underestimates amplitude reduction for all the sources. This may be caused by higher CO_2 saturation than used in the modeling, which used the lower bound of possible saturation to assess detectability levels. At the same time, the traveltime shift computed with equation 2 caused by the same velocity reduction is about 0.35 ms. This reduction is very close to both the modeled and observed traveltime shifts. Taken together, these observations suggest that the average saturation within the CO_2 plume at CRC3 is somewhat higher than 10%, with a plume thickness slightly smaller than 11 m.

For non-zero offset sources, the observed traveltime shifts and amplitude reductions are larger than for the zero offset. For instance, Figure 2 shows that the amplitude change for SOV4 is almost twice that for SOV3, with the rest of sources falling in between. The travetime change is also larger for SOV4 than for SOV3.This is consistent with the modeling and is caused by an oblique angle between the wave propagation direction and the DAS fiber.

Conclusions

The results demonstrate that the proposed approach using DAS to monitor variations of subsurface properties is sensitive to changes of velocity and density in thin layers. Given the borehole length of a DAS cable this technique simultaneously captures seismic attributes in the reservoir and associated overburden. This can be useful in a variety of applications. In particular, in the context of CO_2 storage, it may be used for above-zone monitoring and leakage detection from the target reservoir.

If the density change is insignificant, equations 1 and 2 are a system of two equations with two unknowns (ΔV_P and h), which can both be resolved (similarly to the approach of Ghaderi and Landrø, (2009). Conversely, if the thickness of the formation undergoing changes is known, the approach can resolve changes of ΔV_P and density (if both changes are significant). All three parameters can be resolved by tracking variations of the reflection amplitude (in addition to the direct-wave traveltime shifts and amplitudes).

The approach described above uses permanent seismic sources but can also utilize conventional seismic sources or uncontrolled sources of seismic energy such as earthquakes and human activity (e.g., earth moving equipment).

Acknowledgements

The Otway Project received CO2CRC Ltd funding through its industry members and research partners, the Australian Government under the CCS Flagships Programme, the Victorian State Government and the Global CCS Institute. The authors wish to acknowledge financial assistance provided through Australian National Low Emissions Coal Research and Development. ANLEC R&D is supported by Low Emission Technology Australia (LETA) and the Australian Government through the Department of Industry, Science, Energy and Resources. The authors are grateful to the Otway Stage 3 team colleagues Mohamed Bagheri, Paul Barraclough, Peter Dumesny, Jonathan Ennis-King, Charles Jenkins and Alexey Yurikov for their substantial contribution to the experiment, Michael Mondanos and Stoyan Nikolov (Silixa inc.) for help with the fiber-optic equipment, and Andrej Bóna for insightful discussions.

References

Caspari, E., R. Pevzner, B. Gurevich, T. Dance, J. Ennis-King, Y. Cinar, and M. Lebedev, 2015, Feasibility of CO2 plume detection using 4D seismic: CO2CRC Otway Project case study — Part 1: Rock-physics modeling: Geophysics, **80**, no. 4, B95-B104. http://dx.doi.org/doi:10.1190/geo2014-0459.1.

Cheng, F., J. Correa, S. Dou, B. Freifeld, T. Wood, K. Nihei, D. Guerra, J. Birkholzer, B. Chi, and J. Ajo-Franklin, 2021, Testing of a permanent orbital surface source and distributed acoustic sensing for monitoring of unconventional reservoirs: Preliminary results from the Eagle Ford Shale: Geophysics, **86**, no. 2, P1-P12. http://dx.doi.org/10.1190/geo2020-0403.1.

Correa, J., A. Egorov, K. Tertyshnikov, A. Bona, R. Pevzner, T. Dean, B. Freifeld, and S. Marshall, 2017, Analysis of signal to noise and directivity characteristics of DAS VSP at near and far offsets — A CO2CRC Otway Project data example: The Leading Edge, **36**, no. 12, 994a991-994a997. http://dx.doi.org/10.1190/tle36120994a1.1.

Correa, J., R. Isaenkov, S. Yavuz, A. Yurikov, K. Tertyshnikov, T. Wood, B. M. Freifeld, and R. Pevzner, 2021, Distributed acoustic sensing/surface orbital vibrator: Rotary seismic sources with fiber-optic sensing facilitates autonomous permanent reservoir monitoring: Geophysics, **86**, no. 6, P61-P68. http://dx.doi.org/10.1190/geo2020-0612.1.

Daley, T., B. Freifeld, J. Ajo-Franklin, S. Dou, R. Pevzner, V. Shulakova, S. Kashikar, D. Miller, J. Goetz, J. Henninges, and S. Lueth, 2013, Field testing of fiber-optic distributed acoustic sensing (DAS) for subsurface seismic monitoring: The Leading Edge, **32**, no. 6, 699-706. http://dx.doi.org/doi:10.1190/tle32060699.1.

Davies, K., D. Thornton, J. Stefani, A. Makedonov, and Z. Katrenov. 2020, Fiber Optics for Sub-Surface Strain Forecasting. Paper read at First EAGE Workshop on Fibre Optic Sensing, 9-11 March 2020, at Amsterdam.

Freifeld, B. M., R. Pevzner, S. Dou, T. Daley, M. Robertson, K. Tertyshnikov, T. Wood, J. Ajo-Franklin, M. Urosevic, and B. Gurevich. 2016, The CO2CRC Otway Project deployment of a Distributed Acoustic Sensing Network Coupled with Permanent Rotary Sources. Paper read at 78th EAGE Conference & Exhibition 2016, 30 May - 2 June 2016, at Vienna, Austria.

Galperin, E. I., and J. E. White, 1974, Vertical seismic profiling, Special publication / Society of Exploration Geophysicists: Society of Exploration Geophysicists.

Ghaderi, A., and M. Landrø, 2009, Estimation of thickness and velocity changes of injected carbon dioxide layers from prestack time-lapse seismic data: Geophysics, **74**, no. 2, O17-O28. http://dx.doi.org/10.1190/1.3054659.

Isaenkov, R., R. Pevzner, S. Glubokovskikh, S. Yavuz, A. Yurikov, K. Tertyshnikov, B. Gurevich, J. Correa, T. Wood, B. Freifeld, M. Mondanos, S. Nikolov, and P. Barraclough, 2021, An automated system for continuous monitoring of CO2 geosequestration using multi-well offset VSP with permanent seismic sources and receivers: Stage 3 of the CO2CRC Otway Project: International Journal of Greenhouse Gas Control, **108**, 103317. http://dx.doi.org/10.1016/j.ijggc.2021.103317.

Jenkins, C., P. Barraclough, M. Bagheri, J. Correa, T. Dance, J. Ennis-King, B. Freifeld, S. Glubokovskikh, C. Green, J. Gunning, B. Gurevich, R. Isaenkov, S. Jackson, R. Pevzner, L. Ricard, K. Tertyshnikov, A. Wilkins, T. Wood, S. Yavuz, and A. Yurikov. 2021, Drilling an Array of Monitoring Wells for a CCS Experiment: Lessons From Otway Stage 3 Paper read at Greenhouse Gas Control Technologies Conference 15-18 March 2021, at Online.

Johnson, D. L., 2001, Theory of frequency dependent acoustics in patchy-saturated porous media: Journal of the Acoustical Society of America, **110**, no. 2, 682-694. http://dx.doi.org/Doi:10.1121/1.1381021.

Mateeva, A., and P. M. Zwartjes. 2017, Depth Calibration of DAS VSP Channels: a New Data-Driven Method. Paper read at 79th EAGE Conference and Exhibition 2017, at Paris, France.

Mateeva, A., J. Lopez, D. Chalenski, M. Tatanova, P. Zwartjes, Z. Yang, S. Bakku, K. de Vos, and H. Potters, 2017, 4D DAS VSP as a tool for frequent seismic monitoring in deep water: The Leading Edge, **36**, no. 12, 995-1000. http://dx.doi.org/10.1190/tle36120995.1.

Mavko, G., and T. Mukerji, 1998, Bounds on low-frequency seismic velocities in partially saturated rocks: Geophysics, **63**, no. 3, 918-924. http://dx.doi.org/Doi:10.1190/1.1444402.

Naldrett, G., 2021, A new era of borehole measurements for permanent reservoir monitoring: First Break, **39**, no. 2, 77-81. http://dx.doi.org/10.3997/1365-2397.fb2021014.

Parker, T., A. Gillies, S. Shatalin, and M. Farhadiroushan, 2014, The intelligent distributed acoustic sensing: Proceedings of SPIE - The International Society for Optical Engineering, **9157**. http://dx.doi.org/10.1117/12.2064889.

Pevzner, R., B. Gurevich, A. Pirogova, K. Tertyshnikov, and S. Glubokovskikh, 2020, Repeat well logging using earthquake wave amplitudes measured by distributed acoustic sensors: The Leading Edge, **39**, no. 7, 513-517. http://dx.doi.org/10.1190/tle39070513.1.

Pevzner, R., R. Isaenkov, S. Yavuz, A. Yurikov, K. Tertyshnikov, P. Shashkin, B. Gurevich, J. Correa, S. Glubokovskikh, T. Wood, B. Freifeld, and P. Barraclough, 2021, Seismic monitoring of a small CO2 injection using a multi-well DAS array: Operations and initial results of Stage 3 of the CO2CRC Otway project: International Journal of Greenhouse Gas Control, **110**, 103437. http://dx.doi.org/10.1016/j.ijggc.2021.103437.

Schmidt, H., and F. B. Jensen, 1985, A Full-Wave Solution for Propagation in Multilayered Viscoelastic Media with Application to Gaussian-Beam Reflection at Fluid-Solid Interfaces: Journal of the Acoustical Society of America, **77**, no. 3, 813-825. http://dx.doi.org/Doi 10.1121/1.392050.

Smith, J. O. I., 2007, Mathematics of the Discrete Fourier Transform (DFT): with Audio Applications. 2nd edition ed: W3K Publishing.

Yavuz, S., R. Isaenkov, R. Pevzner, K. Tertyshnikov, A. Yurikov, J. Correa, T. Wood, and B. Freifeld, 2020, Processing of Continuous Vertical Seismic Profile Data Acquired with Distributed Acoustic Sensors and Surface Orbital Vibrators, **2020**, no. 1, 1-5. http://dx.doi.org/10.3997/2214-4609.202070015.

Zhu, T., J. Ajo-Franklin, T. M. Daley, and C. Marone, 2019, Dynamics of geologic CO2 storage and plume motion revealed by seismic coda waves: Proceedings of the National Academy of Sciences, **116**, no. 7, 2464-2469. http://dx.doi.org/10.1073/pnas.1810903116.

Zwartjes, P. M., T. B. Barker, J. C. Hornman, and J. Przybysz-Jarnut. 2015, Quantitative Interpretation of Nine Months of Daily SeisMovie™ Data to Monitor Steam Injection at Schoonebeek. Paper read at 77th EAGE Conference and Exhibition 2015, at Madrid, Spain.

List of figures

Figure 1. Location scheme. CRC-3 is a nearly vertical well instrumented with fiber optic cable cemented behind the casing. Locations of surface orbital vibrators are marked with pink circles. Outer contour of the simulated plume is shown in green.

Figure 2. Left panels: time shifts estimated for each SOV versus depth and survey date. Perforation interval is marked with black dashed horizontal lines, start of the injection with a blue vertical dashed line. Right panels: average traveltime shifts observed post-injection (black) and modeled based on flow simulations for 11 m thick plume (red).

Figure 3. Left panels: relative amplitude change estimated for each SOV versus depth and survey date. Perforation interval is marked with black dashed horizontal lines, start of the injection with blue vertical dashed line. Right panels: average relative amplitude change observed post-injection (black) and modeled based on flow simulations for 11 m thick plume (red).

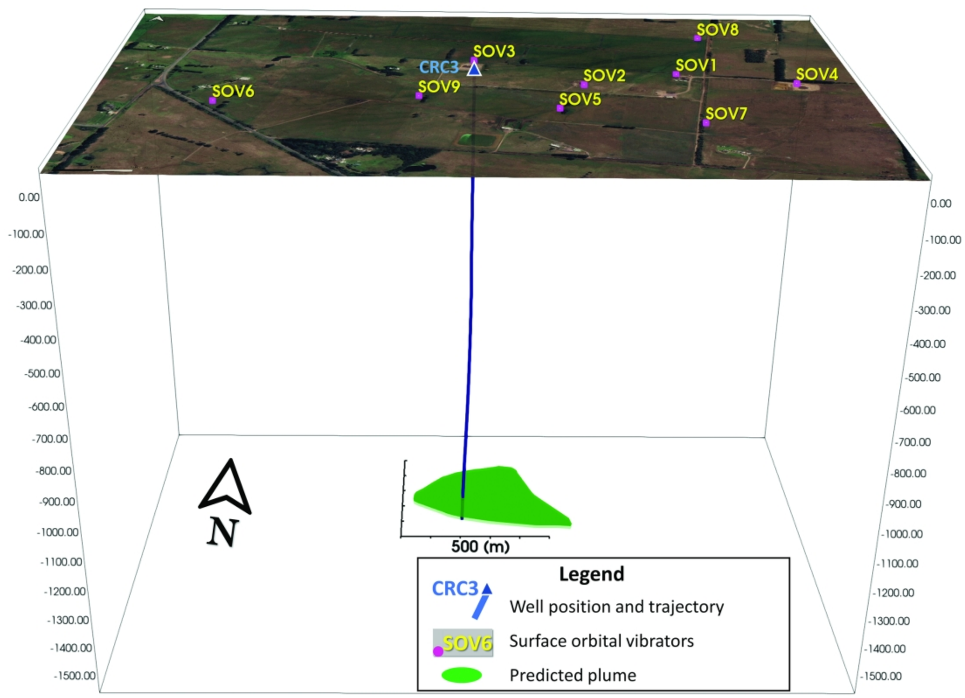

Figure 1. Location scheme. CRC-3 is a nearly vertical well instrumented with fiber optic cable cemented behind the casing. Locations of surface orbital vibrators are marked with pink circles. Outer contour of the simulated plume is shown in green.

222x160mm (300 x 300 DPI)

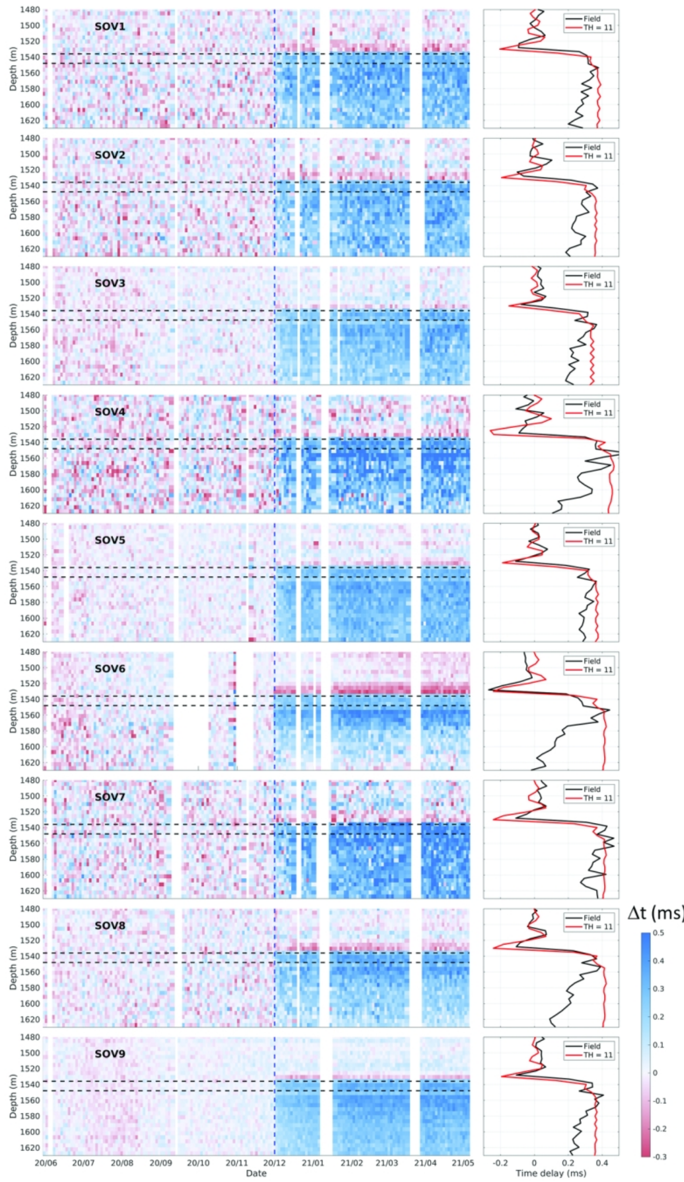

Figure 2. Left panels: time shifts estimated for each SOV versus depth and survey date. Perforation interval is marked with black dashed horizontal lines, start of the injection with a blue vertical dashed line. Right panels: average traveltime shifts observed post-injection (black) and modeled based on flow simulations for 11 m thick plume (red).

100x168mm (300 x 300 DPI)

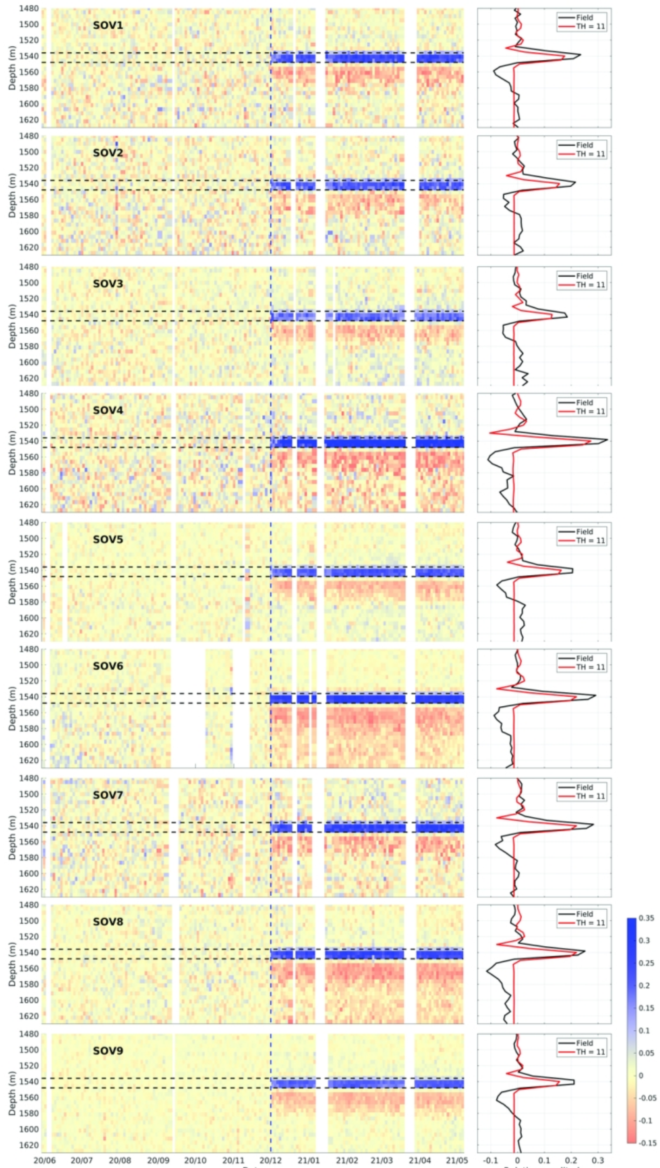

Figure 3. Left panels: relative amplitude change estimated for each SOV versus depth and survey date. Perforation interval is marked with black dashed horizontal lines, start of the injection with blue vertical dashed line. Right panels: average relative amplitude change observed post-injection (black) and modeled based on flow simulations for 11 m thick plume (red).

96x168mm (300 x 300 DPI)

DATA AND MATERIALS AVAILABILITY

Data associated with this research are confidential and cannot be released.

DOI:10.1190/geo2021-0404.1